AN UNUSUAL ASSOCIATION OF HYDROTHERMAL PLATINUM-GROUP MINERALS FROM THE IMANDRA LAYERED COMPLEX, KOLA PENINSULA, NORTHWESTERN RUSSIA

Andrei Y. BARKOV[§] and Michael E. FLEET[§]

Department of Earth Sciences, University of Western Ontario, London, Ontario N6A 5B7, Canada

Abstract

An unusual association of platinum-group minerals (PGM) is observed in a chromitite layer of the Mount Bol'shaya Varaka deposit, Imandra layered complex, Kola Peninsula, Russia. The PGM typically occur as cluster-like or chain-like micro-aggregates, and as separate minute grains located in contact with chromite along grain boundaries. The PGM are enclosed in magnesiohornblende, edenite, talc, or phlogopite, and may transect the host hydrous silicates; they include sperrylite, laurite–erlichmanite, unnamed $Cu_2(Ni,Co)Pt_3S_8$, hollingworthite, pyrite rich in the platinum-group elements (Ru 10.96, Os 0.98, and Ir 0.54 wt.%), nickelian platarsite(?), $(Pt_{0.71}Ni_{0.26}Co_{0.05})_{\Sigma 1.02}As_{1.10}S_{0.88}$, daomanite, and cooperite. Concentrations of Rh and S in the rhodian sulfurian sperrylite vary from 1.0 and 0.8 to 6.6 and 4.9 wt.%, respectively, and the composition most enriched in Rh and S is $(Pt_{0.78}Rh_{0.20}Ir_{0.03})_{\Sigma 1.01}(As_{1.53}S_{0.47})_{\Sigma 2.00}$. The correlations Pt–Rh (correlation coefficient R = –0.99), Pt–As (R = 0.98), Pt–S (R = –0.99), Rh–As (R = –0.97), Rh–S (R = 0.97), and As–S (R = –1.00) are important and consistent with the existence of a new series of solid solution, extending from $PtAs_2$ toward the pyrite-type $Rh_{1-x}S_2$ ("Rh_2S_5"). Most of the PGM precipitated during deuteric alteration at a postmagmatic–hydrothermal stage of crystallization of the chromitite. The majority of the laurite–erlichmanite grains display a close textural relationship with the hydrous silicates and form part of the hydrothermal mineralization at Imandra.

Keywords: platinum-group elements, platinum-group minerals, substitutions, hydrothermal mineralization, chromitite layer, layered intrusion, mafic rocks, Mount Bol'shaya Varaka, Imandra complex, Baltic Shield, Russia.

Sommaire

Nous avons découvert une association inhabituelle de minéraux du groupe du platine (MGP) dans un niveau de chromitite du gisement du Mont Bol'shaya Varaka, complexe stratiforme d'Imandra, péninsule de Kola, en Russie. Les MGP se présentent généralement en micro-aggrégats ou en chaînes, et en grains isolés de taille infime au contact avec la chromite le long des grains. Les MGP sont inclus dans la magnésiohornblende, l'édenite, le talc ou la phlogopite, et peuvent même recouper les silicates hydratés qui les renferment. Parmi les MGP se trouvent sperrylite, laurite–erlichmanite, $Cu_2(Ni,Co)Pt_3S_8$ sans nom, hollingworthite, pyrite riche en éléments du groupe du platine (Ru 10.96, Os 0.98, et Ir 0.54%, poids), platarsite nickelifère (?), $(Pt_{0.71}Ni_{0.26}Co_{0.05})_{\Sigma 1.02}As_{1.10}S_{0.88}$, daomanite, et cooperite. La concentration de Rh et S dans la sperrylite varie de 1.0 et 0.8 à 6.6 et 4.9% (poids), respectivement, et la composition la plus enrichie en Rh et S est $(Pt_{0.78}Rh_{0.20}Ir_{0.03})_{\Sigma 1.01}(As_{1.53}S_{0.47})_{\Sigma 2.00}$. Les corrélations Pt–Rh (coefficient de corrélation R = –0.99), Pt–As (R = 0.98), Pt–S (R = –0.99), Rh–As (R = –0.97), Rh–S (R = 0.97), et As–S (R = –1.00) sont importantes et semblent indiquer l'existence d'une solution solide entre $PtAs_2$ et $Rh_{1-x}S_2$ ("Rh_2S_5") structuralement affiliée à la pyrite. La plupart des MGP se sont formés au cours d'une altération deutérique à un stade postmagmatique hydrothermal de la cristallisation de la chromitite. La majorité des grains de laurite–erlichmanite démontrent un lien textural étroit avec les silicates hydratés et font partie de l'événement d'altération hydrothermale à Imandra.

(Traduit par la Rédaction)

Mots-clés: éléments du groupe du platine, minéraux du groupe du platine, substitutions, minéralisation hydrothermale, niveau de chromitite, intrusion stratiforme, roches mafiques, Mont Bol'shaya Varaka, complexe d'Imandra, bouclier baltique, Russie.

[§]   *E-mail addresses*: abarkov@uwo.ca, mfleet@uwo.ca

INTRODUCTION

The Imandra mafic complex in the Kola Peninsula, northwestern Russia, has an Early Proterozoic age (U– Pb dating of zircon) of 2395 ± 30 Ma (Balashov *et al.* 1990) and 2441 ± 1.6 Ma (Amelin *et al.* 1995). This is one of several related layered intrusions in the Baltic (Fennoscandian) Shield (Fig. 1) that host various depos-

FIG. 1. Generalized geological map of northeastern part of Fennoscandian Shield (based on various sources in the literature), showing the location of the Imandra layered complex.

its of chromite, base-metal sulfides and platinum-group elements, PGE (*e.g.*, Dokuchaeva *et al.* 1985, Barkov *et al.* 1997).

In this paper, we provide a detailed description of an unusual association of platinum-group minerals (PGM) from the Mount Bol'shaya Varaka ("Big Hill") chromitite deposit in the Imandra layered complex, with emphasis on some uncommon or unique PGM and PGE-rich phases. The reported association and genetically indicative textures involving these PGM have important implications for the origin of PGE mineralization associated with chromitites.

GEOLOGICAL BACKGROUND

The Mount Bol'shaya Varaka, Umbarechensky, Mount Devich'ya and some other mafic intrusive bodies (a few to several tens of km across) are exposed in the Lake Imandra area, at the western and southwestern margins of the belt of the Imandra–Varzuga Supergroup of Proterozoic supracrustal rocks (Fig. 1). Dokuchaeva *et al.* (1982, 1985) noted that there is a general similarity in geological structure, geochemistry and mineral compositions among these bodies, and suggested that they are fragments of a pre-existing large lopolith (*ca.* 1500 km^2) that was broken up by subsequent tectonic movements.

The layered series of the Imandra complex has been divided into four zones (Dokuchaeva *et al.* 1982, 1985): (1) The Lower Zone (*ca.* 0.15 km in thickness) composed of alternating layers of plagioclase-bearing pyroxenite, gabbronorite and norite; no olivine-rich cumulates were observed. (2) The Main Zone (*ca.* 2 km in thickness) of homogeneous mesocratic gabbronorite and subordinate melanocratic and leucocratic gabbronorite. (3) The Upper Zone (*ca.* 0.3 km in thickness) of various layers of leucocratic gabbro and anorthosite. The main anorthosite layer (*ca.* 30 m in thickness) is located at the top of this zone. (4) The Uppermost Zone (*ca.* 0.5 km in thickness) of quartz-bearing gabbro and gabbrodiorite. The total thickness of the complex is approximately 3 km. Layers of vanadiferous magnetite occur in the upper zones, and several layers of chromitite are present at the lower stratigraphic levels of the complex (Kozlov *et al.* 1975, Dokuchaeva *et al.* 1985).

MINERALOGY OF THE PGE-BEARING CHROMITITE LAYER FROM THE MOUNT BOL'SHAYA VARAKA DEPOSIT

Chromite and plagioclase

The chromitite layer consists of up to 50 vol.% of chromite grains commonly less than 1 mm in diameter. The chromite grains are locally replaced by abundant rutile (or another polymorph of TiO_2). The mean composition of three grains of chromite (WDS data) is TiO_2 0.66, Al_2O_3 11.41, Cr_2O_3 50.36, V_2O_3 0.38, FeO 28.67,

Fe_2O_3 (calc.) 3.51, MnO 0.60, MgO 3.02, ZnO 0.16, for a total of 98.77 wt.%, corresponding to the formula $(Fe^{2+}_{0.82}Mg_{0.16}Mn_{0.02}Zn_{<0.01})_{\Sigma 1.00}(Cr_{1.39}Al_{0.47}Fe^{3+}_{0.09}Fe^{2+}_{0.02}Ti_{0.02}V_{0.01})_{\Sigma 2.00}O_4$.

Relict igneous plagioclase (probably intercumulus), present in the chromitite, is relatively enriched in the albite component: $An_{52.6-60.4}Ab_{39.6-47.2}Or_{0-0.2}$.

Hydrous silicates

Calcic amphiboles (magnesiohornblende and edenite: Table 1) are the principal hydrous silicates in the chromitite layer. They display very high values of *mg* [*i.e.*, 100 Mg/(Mg + Fe + Mn)], 90.8 to 94.7, and are invariably enriched in Cr (0.6–2.0 wt.% Cr_2O_3). These compositions imply a high-magnesium character for igneous pyroxene in the chromitite; it presumably was a precursor primary mineral for these amphiboles, but is not preserved, even in relics. The calcic amphiboles

TABLE 1. COMPOSITIONS OF AMPHIBOLES FROM THE CHROMITE LAYER OF THE IMANDRA COMPLEX, KOLA PENINSULA, RUSSIA

	1	2	3	4	5	6
SiO_2 wt.%	47.64	52.22	47.11	50.58	54.06	50.94
TiO_2	0.36	0.21	0.23	0.18	0.22	0.11
Al_2O_3	10.65	5.91	12.86	8.66	5.99	8.68
Cr_2O_3	1.56	0.94	0.59	1.73	0.74	2.03
FeO	2.99	2.12	3.22	3.42	2.78	3.39
MnO	0.07	0.10	0.02	n.d.	n.d.	0.16
MgO	19.81	22.38	19.17	19.56	21.16	19.55
NiO	0.30	0.04	n.d.	n.d.	n.d.	n.d.
CaO	12.25	11.88	12.38	12.32	12.70	12.41
Na_2O	1.82	0.99	2.19	1.00	0.72	1.26
K_2O	0.06	0.05	0.17	0.08	0.08	0.17
Cl	0.06	n.d.	n.d.	n.d.	n.d.	n.d.
O≡Cl	0.01	-	-	-	-	-
Total	97.56	96.84	97.94	97.53	98.45	98.70
Si *apfu*	6.69	7.27	6.58	7.05	7.39	7.04
^{IV}Al	1.31	0.73	1.42	0.95	0.61	0.96
^{VI}Al	0.45	0.24	0.70	0.47	0.36	0.45
Cr	0.17	0.10	0.07	0.19	0.08	0.22
Ti	0.04	0.02	0.02	0.02	0.02	0.01
Fe	0.35	0.25	0.38	0.40	0.32	0.39
Mn	<0.01	0.01	<0.01	-	-	0.02
Mg	4.15	4.64	3.99	4.06	4.32	4.03
Ni	0.03	<0.01	-	-	-	-
Ca	1.84	1.77	1.85	1.84	1.86	1.84
Na	0.50	0.27	0.59	0.27	0.19	0.34
K	0.01	<0.01	0.03	0.01	0.01	0.03
Cl	0.01	-	-	-	-	-
mg	92.22	94.70	91.30	91.03	93.10	90.77

Columns 1 to 3: results of WDS electron-microprobe analyses (JEOL–733 microprobe). 4 to 6: results of quantitative SEM/EDS electron-microprobe analyses. Numbers 1 and 2: host for two grains of PGE-rich pyrite and associated PGM (Fig. 3). 4 and 5: host for a micro-aggregate of PGM (Figs. 2A-D). 6: amphibole that forms an intergrowth with phlogopite: SiO_2 41.38, TiO_2 1.17, Al_2O_3 18.49, Cr_2O_3 2.10, FeO 2.50, MgO 24.37, Na_2O 0.69, and K_2O 8.51, Total 99.21 wt.%: results of SEM/EDS analysis. These amphibole and phlogopite are the host for a micro-aggregate of PGM, which consists of hollingworthite, sperrylite, laurite, and platarsite(?). All Fe is expressed as FeO (wt.%). F was not detected. n.d.: not detected. The formulae were calculated on the basis of O = 23. *mg* = 100 Mg/(Mg + Fe + Mn).

are devoid of Cl or contain only trace amounts of Cl (Table 1), consistent with the crystallochemical constraints of the Mg–Cl avoidance principle discussed in Oberti *et al.* (1993). Talc also seems to be a replacement product of pyroxene. It is associated with the calcic amphiboles and phlogopite, and has the composition (EDS data) SiO_2 63.19, MgO 30.73, FeO 0.94, Al_2O_3 0.59, and total 95.45 wt.%, corresponding to a formula of $(Mg_{2.90}Fe_{0.05})_{\Sigma2.95}(Si_{3.99}Al_{0.04})_{\Sigma4.03}O_{10}(OH)_2$. Phlogopite is common in the chromitite layer. Its composition is close to end-member phlogopite (MgO 24.0–24.4, FeO 2.0–2.5 wt.%), and is characterized by elevated contents of Cr (0.9 –2.1 wt.% Cr_2O_3), Ti (1.1–1.2%), and Na (0.6–0.7% Na_2O).

Cl-rich apatite

Apatite is a common accessory mineral in the chromitite. It is interstitial with respect to chromite, typically occurring as subhedral to anhedral grains up to 0.1–0.2 mm in maximum dimension, and invariably containing elevated levels of Cl. A grain of Cl-rich apatite is present in the same polished section as a micro-aggregate of PGM (Figs. 2A–D), and contains up to 3.45 wt.% Cl (*i.e.*, 0.49 Cl atoms per formula unit, *apfu*).

Baddeleyite and zircon

Accessory baddeleyite (up to *ca.* 0.2 mm in length) is enclosed by hydrous silicates and mantled by a nar-
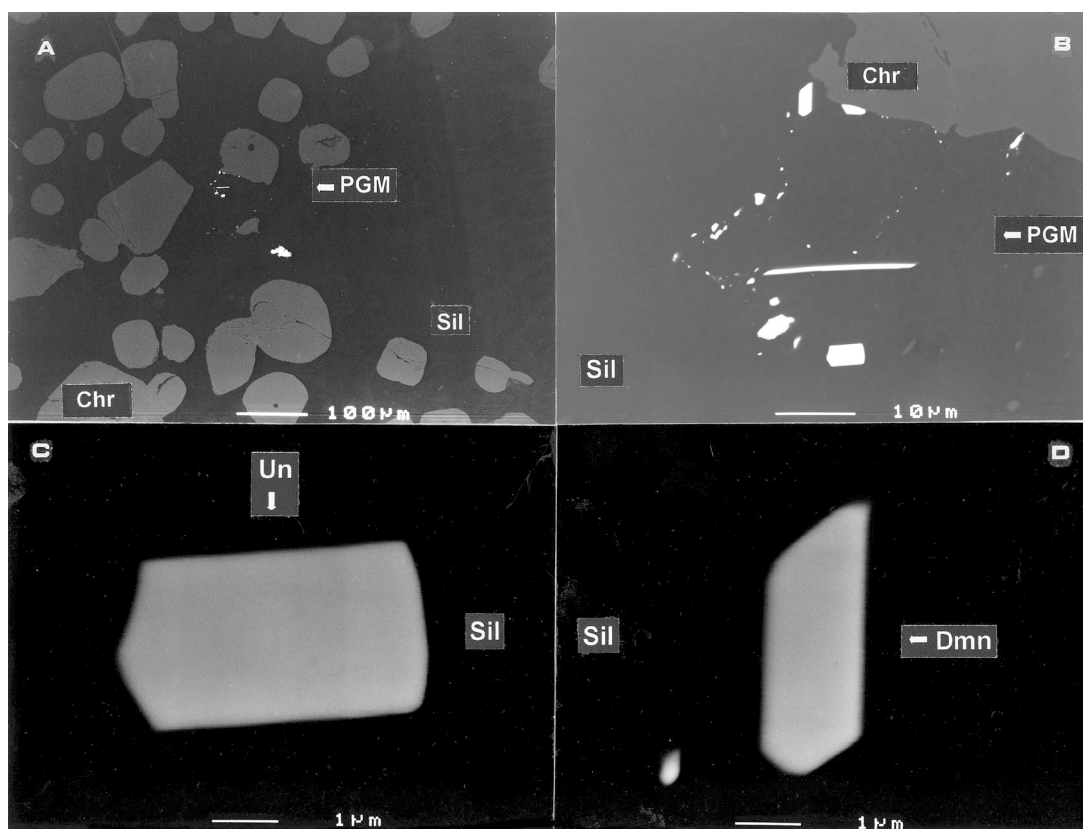

FIG. 2.   A. Micro-aggregate of various platinum-group minerals (PGM: white) enclosed within hydrous silicates: magnesian calcic amphiboles and talc (Sil). Chr: chromite. B. Magnification of the micro-aggregate (shown in Fig. 2A), which consists of sperrylite, unnamed $Cu_2(Ni,Co)Pt_3S_8$ and daomanite, and displays the chain-like morphology. Sil: the host magnesiohornblende (anal. 4, Table 1). C and D: Further magnification of this micro-aggregate, showing subhedral crystals of unnamed $Cu_2(Ni,Co)Pt_3S_8$ (Un) and daomanite (Dmn) enclosed within the hydrous silicates (Sil). Back-scattered electron images.

row rim of zircon, which is likely a consequence of the build-up of SiO_2 in the interstitial fluid, resulting in a reaction of the type $ZrO_2 + SiO_2 = ZrSiO_4$. The baddeleyite contains up to 2.0% HfO_2 and 0.6% TiO_2.

Base-metal sulfides

Chalcopyrite, bornite, millerite, pyrite, and pentlandite form single grains (typically up to 50 μm) or mutual intergrowths. These sulfides are scarce and typically enclosed by hydrous silicates, but they are occasionally present as inclusions within chromite. Two grains of chalcopyrite contain Cu 33.67 and 33.92, Fe 31.05 and 30.71, S 34.62 and 34.86, and total 99.34 and 99.49 wt.%, with formulae represented by $Cu_{0.98}Fe_{1.01-1.03}S_{1.99-2.00}$, and thus are more consistent with chalcopyrite than with any of the known chalcopyrite-derivative minerals: mooihoekite, talnakhite or putoranite. A representative composition of bornite is Cu 61.74, Fe 10.55, S 26.09, and total 98.38 wt.%, with a formula $Cu_{4.92}Fe_{0.96}S_{4.12}$. The composition of millerite is Ni 63.88, Fe 0.66, S 36.17, and total 100.71 wt.%, with a formula $(Ni_{0.98}Fe_{0.01})_{\Sigma 0.99}S_{1.01}$. Pyrite contains minor amounts of Ni or Co; compositions of two grains are Fe 46.17 and 46.14, Ni 0.83 and 0.0, Co 0.0 and 0.81, S 53.87 and 53.05, and total 100.87 and 100.0 wt.%, corresponding to formulae in the range $(Fe_{0.98-0.99}Ni_{0.02-0.0}Co_{0.0-0.02})_{\Sigma 1.00-1.01}S_{2.00-1.99}$, respectively. Pentlandite is strongly enriched in Ni: Fe 23.45, Ni 43.72, S 33.41, total 100.58 wt.%, with a formula $(Ni_{5.74}Fe_{3.24})_{\Sigma 8.98}S_{8.03}$.

PLATINUM-GROUP MINERALS FROM THE CHROMITITE LAYER

The laurite–erlichmanite series

The compositions of laurite–erlichmanite in the chromitite vary from $(Ru_{0.90}Os_{0.06}Ir_{0.03})_{\Sigma 0.99}S_2$ to $(Os_{0.63}Ru_{0.23}Ir_{0.08})_{\Sigma 0.94}S_2$. Members of the laurite–erlichmanite series occur in two distinct textural associations: (1) they are dominantly located at the contact of chromite grains with the hydrous silicates or are enclosed within these hydrous silicates. The largest grain of laurite, which is euhedral and *ca.* 20 μm in size, occurs at the outer contact of chromite and displays compositional zoning: Ru is enriched in the core and Os at the edge of the grain. (2) Micro-inclusions of laurite–erlichmanite in chromite are also quite common, but these are less abundant than the laurite grains associated with the hydrous silicates.

Submicrometric laurite (less than 0.5 μm in size) occurs in close association with ruthenian pyrite (Fig. 3), and these PGM are enclosed by magnesiohornblende (anal. 2, Table 1). Laurite in this association was recognized on the basis of results of SEM/EDS analyses,
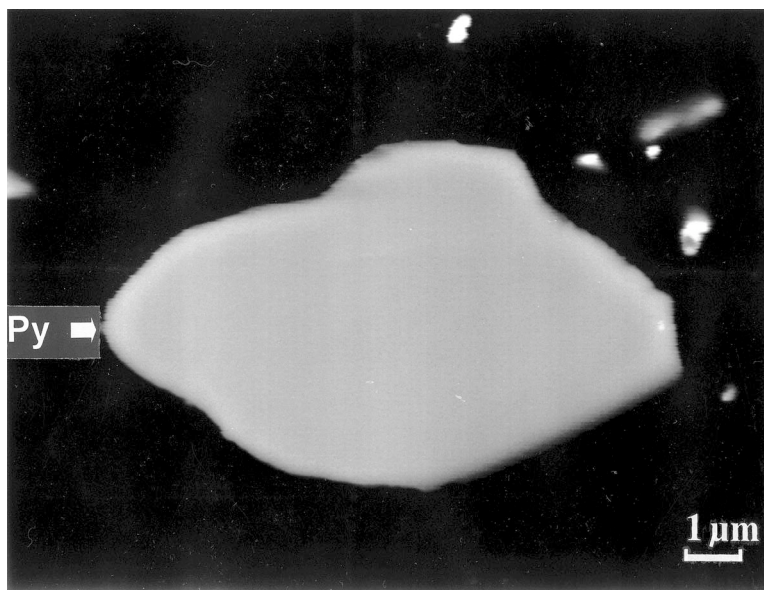

FIG. 3. Anhedral PGE-rich pyrite (Py) enclosed within calcic amphibole: black (magnesiohornblende: anal. 2, Table 1). The associated PGM grains, which are bright white and less than 1 μm in size (near the pyrite: upper right), are laurite (semi-quantitative SEM/EDS data). Back-scattered electron image. The scale bar equals 1 μm.

which are useful in spite of their low totals; such grains yielded a laurite-type formula (*e.g.*, $Ru_{0.93}S_{2.07}$). The submicrometric laurite–erlichmanite also forms part of cluster-like micro-aggregates of the PGM in the Mg-rich calcic amphiboles, and is closely associated with hollingworthite, sperrylite, unnamed $Cu_2(Ni,Co)Pt_3S_8$, and chalcopyrite.

Rhodian sulfurian sperrylite

Sperrylite is relatively common and occurs as submicrometric grains closely associated with the other PGM and with the hydrous silicates. For example, four grains of sperrylite are present in the micro-aggregate shown in Figure 2B. Occurrences of submicrometric $PtAs_2$ are known in other Mg-rich environments, *e.g.*, in komatiitic basalts of the Abitibi greenstone belt, Canada (Stone *et al.* 1996).

The rhodian sulfurian variety of sperrylite is very rare; only a few grains were observed. Results of a detailed study (SEM/EDS) of the largest of these grains, enclosed within talc (Fig. 4), are listed in Table 2. Most of these compositions pertain to a part of the grain (shown by the white arrow in Fig. 4) that is homogeneous and devoid of inclusions. Thus, Rh and S are believed to be present in solid solution. These compositions are in excellent agreement with the sperrylite-type formula $(Pt,Rh)(As,S)_2$, and display covariations in Pt, Rh, As and S (Table 2). The amount of Pt correlates

TABLE 2. COMPOSITIONS OF RHODIAN SULFURIAN SPERRYLITE FROM THE IMANDRA COMPLEX, KOLA PENINSULA, RUSSIA

	Pt	Rh	Ir	As	S	Total
1	49.50	6.61	1.61	37.38	4.90	100.00
2	49.87	5.98	1.87	37.79	4.48	99.99
3	50.19	5.83	1.02	38.87	4.10	100.01
4	50.54	5.42	2.09	37.76	4.19	100.00
5	50.76	5.33	1.72	38.06	4.13	100.00
6	51.07	4.86	1.86	38.18	4.03	100.00
7	50.87	4.93	2.04	38.38	3.78	100.00
8	51.26	4.73	1.82	38.73	3.45	99.99
9	51.94	4.51	1.51	38.42	3.62	100.00
10	50.92	4.68	2.04	38.69	3.67	100.00
11	51.15	4.50	2.30	38.64	3.41	100.00
12	51.55	4.24	2.11	38.84	3.26	100.00
13	51.57	4.22	2.08	38.80	3.33	100.00
14	55.24	2.24	n.d.	41.54	0.98	100.00
15	57.15	0.99	n.d.	41.09	0.77	100.00
	Pt	Rh	Ir	ΣMe	As	S
1	0.779	0.197	0.026	1.002	1.531	0.469
2	0.794	0.180	0.030	1.004	1.566	0.434
3	0.796	0.175	0.016	0.987	1.605	0.395
4	0.816	0.166	0.034	1.016	1.588	0.412
5	0.817	0.163	0.028	1.008	1.595	0.405
6	0.824	0.149	0.030	1.003	1.604	0.396
7	0.828	0.152	0.034	1.014	1.626	0.374
8	0.841	0.147	0.030	1.018	1.655	0.345
9	0.851	0.140	0.025	1.016	1.639	0.361
10	0.828	0.144	0.034	1.006	1.637	0.363
11	0.843	0.141	0.038	1.022	1.658	0.342
12	0.852	0.133	0.035	1.020	1.672	0.328
13	0.850	0.132	0.035	1.017	1.666	0.334
14	0.968	0.074	-	1.042	1.896	0.104
15	1.024	0.034	-	1.058	1.916	0.084

The analytical data (results of quantitative SEM/EDS analyses) are first listed in wt.%, then are shown in terms of atom proportions, based on a total (S + As) of 2 atoms per formula unit.
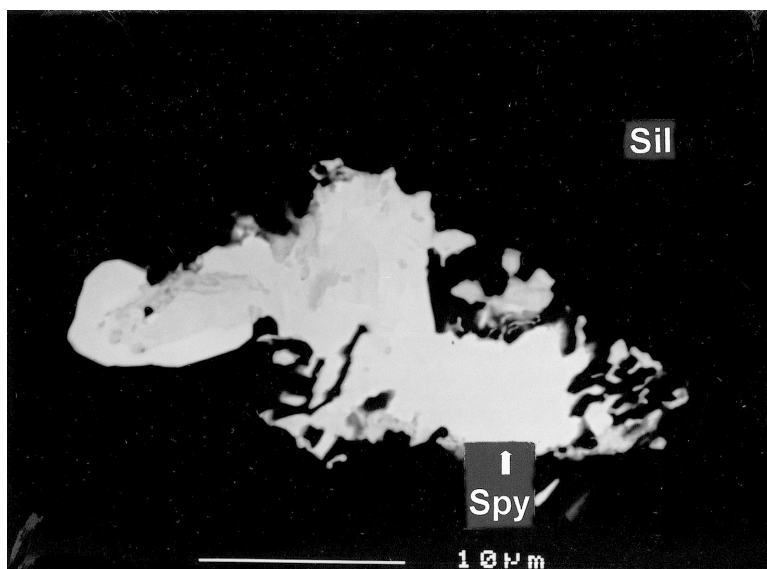

FIG. 4. Anhedral grain of rhodian sulfurian sperrylite (Spy), which is enclosed within talc (Sil), near its contact with a magnesiohornblende (anal. 5, Table 1). Back-scattered electron image.

strongly and negatively with that of Rh (correlation coefficient $R = -0.99$: Fig. 5A) and positively with As ($R = 0.98$: Fig. 5B). The Pt–S correlation is strong and negative: $R = -0.99$ (Fig. 5C). In contrast, the amount of Rh correlates negatively with that of As ($R = -0.97$: Fig. 5D) and positively with S ($R = 0.97$: Fig. 5E). The As–S correlation is inverse: $R = -1.00$ (Fig. 5F). These variations (Figs. 5A–F) are quite distinct from those observed in the sperrylite–hollingworthite series from the Nomgon complex, Mongolia (Izokh & Mayorova 1990). In addition, a strong grain-to-grain variation in the amount of Rh and S was observed in the sperrylite–hollingworthite; in contrast, individual grains of these

sulfarsenides at Nomgon are not zoned and contain uniform levels of Rh and S (Izokh & Mayorova 1990). These observations imply that Rh and S occur in solid solution.

Unnamed $Cu_2(Ni,Co)Pt_3S_8$

An average composition of this complex chalcogenide can be recalculated to the formula $Cu_2(Ni,Co)$ Pt_3S_8 (Table 3). This phase occurs as tiny grains (up to 7 μm in longest dimension), both anhedral and subhedral, enclosed by magnesian calcic amphibole(s) or located at the contact of chromite and hydrous silicate grains. In addition, unnamed $Cu_2(Ni,Co)Pt_3S_8$ is
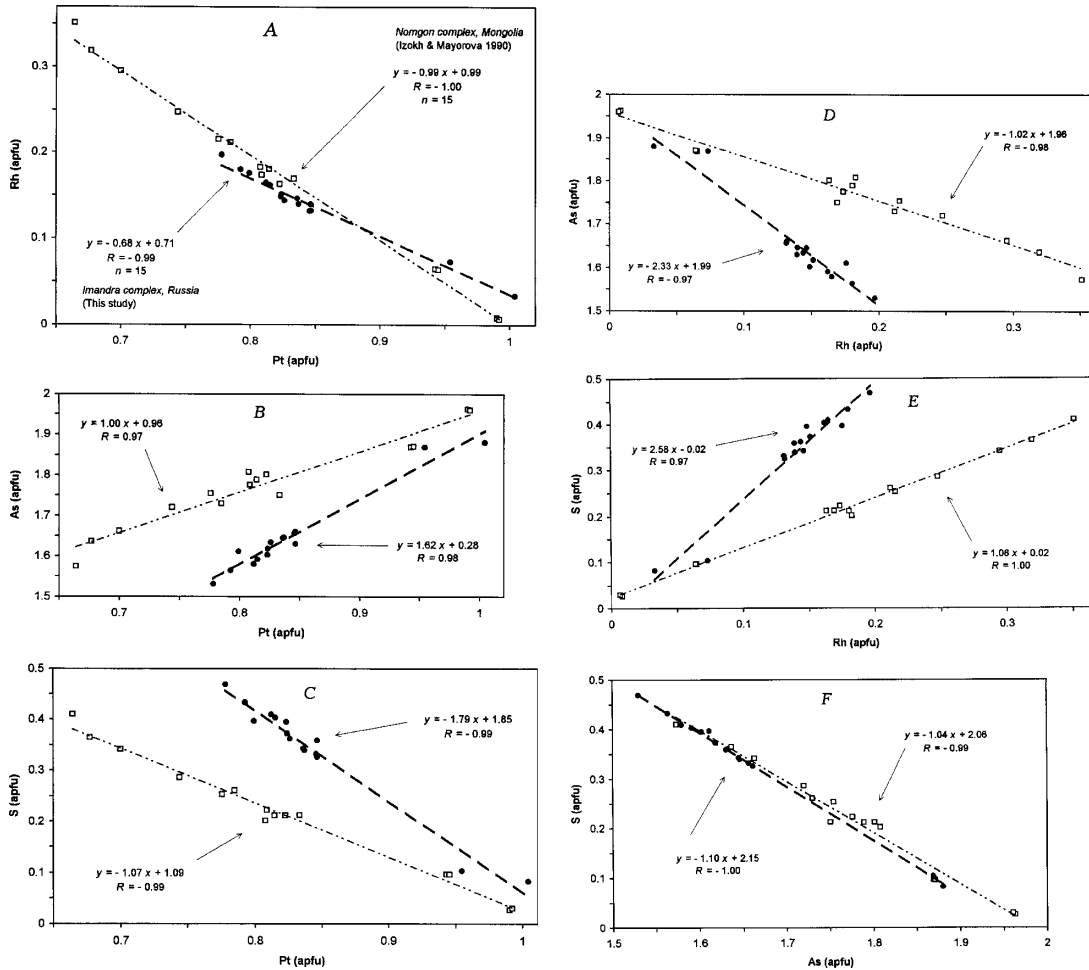

FIG. 5.   (A–F). Correlation of Pt and Rh (A), Pt and As (B), Pt and S (C), Rh and As (D), Rh and S (E), and of As and S (F) (in atoms per formula unit, *apfu*: Σ atoms = 3) in EMPA compositions of rhodian sulfurian sperrylite from the Imandra complex (filled symbol: this study). Compositions of the sperrylite–hollingworthite series from the Nomgon complex, Mongolia, also are plotted for comparison [open symbol: compositions after Izokh & Mayorova (1990). The trends, regressions and values of correlation coefficients *R* shown on these plots: this study].

present in micro-aggregates among the other PGM (*e.g.*, Figs. 2B, C).

PGE-rich pyrite

The average composition of PGE-rich pyrite (Fig. 3) is Fe 35.74, Ru 10.96, Os 0.98, Ir 0.54, S 51.71, for a total of 99.93 wt.%, which corresponds to the formula $(Fe_{0.81}Ru_{0.14}Os_{0.007}Ir_{0.004})_{\Sigma 0.96}S_{2.04}$ (WDS data; JEOL–733 microprobe: this study). Pt and As were not detected (minimum detection-limits: ≤ 0.1 wt.%).

Hollingworthite

Hollingworthite commonly occurs as submicrometric grains (less than 5 μm) among cluster- and chain-like micro-aggregates of PGM enclosed in hydrous silicates. Typically, it is close to stoichiometric RhAsS in composition: *e.g.*, Rh 47.84, Pt 0.49, Ir not detected, As 36.15, S 15.52, and total 100.0 wt.%, with a formula $(Rh_{0.97}Pt_{<0.01})_{\Sigma 0.97}As_{1.01}S_{1.01}$.

Nickelian platarsite (?)

Tiny grains (up to 15 μm long) of a Pt–Ni sulfarsenide occur at the contact of chromite with hydrous silicates or are enclosed within them. Such grains may contain unidentifiable micro-inclusions, and there are signs of a late alteration of these grains along their contact with the host silicates. A part of such grain, which is 3 × 2 μm in size, was analyzed (SEM/EDS). This area appears quite homogeneous in back-scattered electron imaging and consists of a secondary Pt–Ni sulfarsenide, probably nickelian platarsite of composition Pt 52.51, Ni 5.75, Co 1.10, S 10.66, As 31.34, and total 101.36 wt.%. The corresponding formula is $(Pt_{0.71}Ni_{0.26}Co_{0.05})_{\Sigma 1.02}As_{1.10}S_{0.88}$, which implies the existence of a solid solution between platarsite (PtAsS) and gersdorffite–cobaltite (Ni,Co)AsS. An excess in As

is observed in this phase, relative to the As:S ratio of 1.00, and is consistent with the presence of a minor component of $NiAs_2$ (rammelsbergite or pararammelsbergite), which is quite common in natural and synthetic gersdorffite. Alternatively, this increase in the As:S ratio points to the presence of the sperrylite ($PtAs_2$) component.

Daomanite

Daomanite is present as rare submicrometric subhedral grains enclosed by hydrous silicates (Fig. 2D). Its composition agrees very well with the ideal formula $PtCuAsS_2$, and is consistent with the existence of a minor substitution of Pt for Cu (Table 4). This occurrence of daomanite at Imandra is the only reported locality outside China, where it occurs in Cu–Co–(Pt)-rich veins enriched in bornite and chalcopyrite associated with a garnet amphibole pyroxenite and olivine pyroxenite (Yu 1986, 2001, Tin *et al.* 1981). Yu *et al.* (1978) proposed that daomanite could have formed by the replacement of bornite. This mode of formation is very unlikely for the subhedral daomanite from Imandra (Fig. 2D).

Cooperite

A subhedral crystal of cooperite (*ca.* 5 μm in the longest dimension) occurs at the contact of chromite with a hydrous silicate and has the composition Pt 82.78, Pd 1.31, Ni 0.53, S 14.76, and total 99.38 wt.%, corresponding to a formula of $(Pt_{0.94}Pd_{0.03}Ni_{0.02})_{\Sigma 0.99}S_{1.02}$.

Isoferroplatinum or ferroan platinum

A Pt_3Fe-type alloy (<5 μm in size), either isoferroplatinum or ferroan platinum, forms an intergrowth with laurite–erlichmanite, within grains of chromite. The composition of this alloy is Pt 88.88, Rh 1.92, Fe 9.20, for a total of 100.0 wt.%, and the formula is $(Pt_{2.85}Rh_{0.12})_{\Sigma 2.97}Fe_{1.03}$. The identification requires powder X-ray-diffraction data (Cabri & Feather 1975), which could not be obtained owing to its small grain-size.

TABLE 3. AVERAGE COMPOSITION OF UNNAMED $Cu_3(Ni,Co)Pt_3S_8$ FROM THE IMANDRA LAYERED COMPLEX, KOLA PENINSULA, RUSSIA

	Average[§]	Range[§]	Atom proportions	
Pt wt.%	53.56	49.87 – 56.64	Cu *apfu*	1.93
Rh	1.85	0 – 4.28	Fe	0.07
Ir	0.94	0 – 2.43	*Σ*	*2.00*
Cu	12.10	11.04 – 12.40	Ni	0.74
Ni	4.27	3.47 – 4.91	Co	0.17
Co	1.01	0.8 – 1.63	Fe	0.08
Fe	0.82	0.5 – 1.03	*Σ*	*0.99*
S	25.19	24.36 – 25.71	Pt	2.79
			Rh	0.18
Total	99.74		Ir	0.05
			Σ	*3.02*
			S	7.98

[§] The average composition and the ranges are results of seven electron-microprobe analyses. The atom proportions are based on a total of 14 atoms per formula unit (*apfu*).

TABLE 4. COMPOSITION OF DAOMANITE FROM THE IMANDRA COMPLEX, KOLA PENINSULA, RUSSIA

	Pt	Cu	As	S	Total
1 wt.%	51.51	14.31	18.36	15.38	99.56
2	50.49	14.87	18.32	16.44	100.12
1 apfu	1.09	0.93	1.01	1.98	
2	1.04	0.94	0.98	2.05	

1: Daomanite from the Imandra complex, Russia (this study).
2: Daomanite from the Yanshan region, China (Yu 1986).
Atom proportions are based on a total of 5 atoms per formula unit (*apfu*).

DISCUSSION AND CONCLUSIONS

Implications from the occurrence of rhodian sulfurian sperrylite

The composition of sperrylite is typically close to $PtAs_2$ (*e.g.*, Cabri & Laflamme 1981). Although minor Rh and S may substitute for Pt and As, respectively, the presence of high contents of these elements and their covariations in sperrylite are highly unusual. The existence of a S-for-As substitution is consistent with the experimental findings of Makovicky *et al.* (1992): in the system Pt–Fe–As–S, sperrylite contains up to 25.3 at.% S at 850°C and 23 at.% S at 470°C substituting for As.

The compositional series observed at Imandra differs markedly from the series reported from the Nomgon complex in Mongolia (Izokh & Mayorova 1990), which is the only other reported occurrence of rhodian sulfurian sperrylite. The compositions (Table 2, Figs. 5A–F) suggest the existence at Imandra of a new solid-solution series, extending from nearly end-member sperrylite ($PtAs_2$) toward Rh_2S_5 or RhS_3, with a pyrite-type or related structure. The phase Rh_2S_5 has been synthesized by reaction of $RhCl_3$ with S at 600°C (Wohler *et al.* 1933). The powder X-ray-diffraction pattern of Rh_2S_5 was reported to be of a "pseudopyrite type" and is similar to that of pyrite (Juza *et al.* 1935). More recently, the pyrite-type phase in the binary system Rh–S was reported to be of RhS_3 composition ($a = 5.58$ Å: Berlincourt *et al.* 1981). Also, Makovicky *et al.* (2002) reported that in the system Fe–Rh–S at 900 and 500°C, the RhS_3 pyrite phase has the actual composition $Rh_{2.75}S_{7.25}$, which has a Rh:S ratio (0.38) closer to Rh_2S_5 (0.40) than to RhS_3 (0.33). Thus, further experimental work is needed to determine the actual composition or the range of composition of the pyrite-type phase in the system Rh–S. We note that the compositional series of the rhodian sulfurian sperrylite at Imandra extends toward "Rh_2S_5" rather than toward "RhS_3" (Table 2).

The occurrence of rhodian sulfurian sperrylite at Imandra is consistent with the existence of other solid-solution series that involve sperrylite and pyrite-type compounds. The sperrylite–geversite ($PtSb_2$) solid solution was reported from the Owendale complex in Australia (Johan *et al.* 1989), and is presumably related to the synthetic $PtAs_{2-x}Sb_x$ solid solution (Furuseth *et al.* 1967). A limited extent of solid solution exists between sperrylite and erlichmanite, OsS_2 (Tolstykh *et al.* 2002).

Substitutions and crystal-chemical implications

The substitution of Rh for Pt in the rhodian sulfurian sperrylite at Imandra appears to be controlled and charge-compensated by a S-for-As substitution. The charge-balance mechanism $Rh^{3+} + (AsS)^{3-} = Pt^{4+} + (As_2)^{4-}$ was suggested for the incorporation of Rh in the sperrylite–hollingworthite series (Barkov *et al.* 1999b). However, the electronic structure of $PtAs_2$ is not well understood, and an alternative scheme $Rh^{3+} + (AsS)^{3-} = Pt^{2+} + (As_2)^{2-}$ may be suggested instead. The compositional data for this PGM from the Nomgon complex, Mongolia, agree very well with this substitution model (Figs. 5A–F). However, the present results for rhodian sulfurian sperrylite from the Imandra complex (Table 2) point to the substitution [Rh + 2S = Pt + 2As]. On the other hand, the pyrite-type structure is consistent with the presence of $(S_2)^{2-}$ dumbbells, and pure RhS_2 does not exist in the Rh–S system (Hulliger 1964). As discussed above, the Rh–S and Fe–Rh–S phase relations suggest that this solid solution should extend to "Rh_2S_5" ("$Rh_{2.75}S_{7.25}$") or, alternatively, to "RhS_3". In this case, the overall charge-compensation can be achieved by omission of Rh atoms. We note that ΣMe decreases with increase in Rh (and S), in approximate agreement with this model (Table 2). Formulae of the pyrite-type phase of Rh may be represented as $Rh_{0.8}S_2$ (*i.e.*, "Rh_2S_5" and "$Rh_{2.75}S_{7.25}$") and $Rh_{0.67}S_2$ ("RhS_3").

They are consistent with two mechanisms of substitution that assume the presence of vacancies: (*1*) [0.4 Rh^{3+} + 0.4 Rh^{2+} + 0.2 $^{Me}\square$ + $(S_2)^{2-}$ = Pt^{2+} + $(As_2)^{2-}$] and (*2*) [0.667 Rh^{3+} + 0.333 $^{Me}\square$ + $(S_2)^{2-}$ = Pt^{2+} + $(As_2)^{2-}$], respectively. The present model implies that the likely formula of the pyrite-type phase in the system Rh–S is $Rh_{1-x}S_2$, rather than "Rh_2S_5" or "RhS_3". In addition, substitution scheme 1 assumes the mixed-valence character of the pyrite-type $Rh_{1-x}S_2$ phase, *i.e.*, $Rh^{3+}_{0.4}$ $Rh^{2+}_{0.4}S_2$ with a ratio Rh^{2+} : Rh^{3+} of 1 : 1.

Our data indicate that substantial amounts of Ru, Os and Ir can be incorporated in pyrite, which forms a solid solution toward laurite–erlichmanite (which is isostructural with pyrite), according to the homovalent scheme $[(Ru, Os)^{2+} = Fe^{2+}]$. This is the only reported occurrence of natural $Fe_x(Ru,Os)_{1-x}S_2$ solid solution. The related phases of the $Fe_xRu_{1-x}S_2$ type with $x = 0.1, 0.2, 0.3, 0.5$, and 0.9 have been synthesized by Hwang *et al.* (1994) using oscillating chemical vapor transport. The presence of Ir (0.54 wt.%) in the ruthenoan pyrite at Imandra is consistent with a solid-solution series extending toward the pyrite-type $Ir_{1-x}S_2$ phase.

The observed solid-solution in platarsite toward gersdorffite–(cobaltite) at Imandra must have been facilitated by the structural similarities between these two members of the cobaltite group. Platarsite has the ideal formula of PtAsS (Cabri *et al.* 1977, Cabri 2002). We assume that platarsite is a mixed-valence compound: $Pt^{4+}_{0.5}Pt^{2+}_{0.5}[AsS]^{3-}$. The incorporation of Me^{3+} (*e.g.*, Rh, Ir or Ni) in platarsite could be thus governed by the heterovalent substitution $2Me^{3+} = (Pt^{4+} + Pt^{2+})$. The presence of a minor diarsenide (As_2^{4-}) component in the composition of nickelian platarsite at Imandra implies a corresponding increase in Pt^{4+} relative to Pt^{2+} in order to maintain charge balance.

*Unnamed Cu$_2$(Ni,Co)Pt$_3$S$_8$
and related synthetic phases*

This complex chalcogenide is similar to thiospinels in composition (Table 3), and its formula might be written as (Cu$_{0.97}$Fe$_{0.04}$)$_{\Sigma 1.04}$(Pt$_{1.39}$Ni$_{0.37}$Rh$_{0.09}$Co$_{0.09}$ Ir$_{0.02}$)$_{\Sigma 1.96}$S$_{3.99}$ (Σ atoms = 7) or, ideally, Cu(Pt,Ni)$_2$S$_4$. Therefore, this PGM was initially reported as "nickeloan malanite" (Barkov *et al.* 1997). A revised formula of Cu$_2$(Ni,Co)Pt$_3$S$_8$ is suggested in Table 3 by analogy with synthetic Cu$^+_2$Pt^{2+}Pt$^{4+}_3$S$_8$, which is monoclinic, space group *P*2/*n* (Gross & Jansen 1994). This revision of the ideal formula is consistent with the following observations: (1) It is known that natural thiospinels of Cu and PGE form very broad ranges of mutual solid-solutions in the system CuRh$_2$S$_4$–CuIr$_2$S$_4$–CuPt$_2$S$_4$. However, thiospinels close to end-member CuPt$_2$S$_4$ are lacking (*e.g.*, Barkov *et al.* 1997 and references therein). (2) No synthetic CuPt$_2$S$_4$ having a spinel-type structure has been reported; instead, monoclinic Cu$_2$Pt$_4$S$_8$ occurs at this ideal composition (Gross & Jansen 1994). In contrast, the thiospinels CuRh$_2$S$_4$ and CuIr$_2$S$_4$ have been synthesized and are characterized widely in the literature. Thus, a miscibility gap may exist close to CuPt$_2$S$_4$ in the system CuRh$_2$S$_4$–CuIr$_2$S$_4$–CuPt$_2$S$_4$. (3) The content of Pt in the unnamed phase at Imandra is 2.8 *apfu* (Table 3), which is close to 3 Pt^{4+} *apfu* in monoclinic Cu$^+_2$Pt^{2+}Pt$^{4+}_3$S$_8$. This correspondence implies that Ni^{2+} and Co^{2+} substitute for Pt^{2+} in the Imandra phase, and that the likely structural formula is Cu$^+_2$(Ni,Co)$^{2+}$ Pt$^{4+}_3$S$_8$.

In the absence of structural data, the reported synthetic phases CuPt$_2$S$_4$ (Evstigneeva 1994) and Cu(Pt, Ni)$_2$S$_4$ (Peregoedova & Ohnenstetter 2002) may be, in fact, monoclinic Cu$_2$Pt$_4$S$_8$ and Cu$_2$Pt$_{3-x}$(Ni,Fe)$_{1+x}$S$_8$, and related to the monoclinic copper thioplatinate of Gross & Jansen (1994). It is noteworthy that the composition of the PGM (two grains) in Peregoedova & Ohnenstetter (2002) is (Cu$_{1.83}$Fe$_{0.17}$)$_{\Sigma 2.00}$[Pt$_{2.66}$(Ni$_{1.37}$Fe$_{0.12}$)$_{1.49}$]$_{\Sigma 4.15}$ S$_{7.85}$ and Cu$_{2.08}$[Pt$_{2.54}$(Ni$_{1.13}$Fe$_{0.49}$)$_{1.62}$]$_{\Sigma 4.16}$S$_{7.76}$, so that the Pt content is close to 3 *apfu*, as in the phase from the Imandra complex (Table 3).

Genetic implications

Most of the PGM species observed in the Bol'shaya Varaka deposit are rich in Pt, Ru and Rh in proportions consistent with the general trend of PGE abundance in the chromitite, *i.e.*, Pt $\geq$ Ru > Rh. No Pd-based species have been found. The following features of the PGE mineralization at Bol'shaya Varaka are observed: (1) The PGE occur as minute and discrete species of PGM (typically $\leq$5 μm) in association with hydrous silicates, chromite and base-metal sulfides. (2) The very low amounts of the base-metal sulfides and their very small grain-size indicate that bulk concentrations of S are very low in the chromitite. (3) With the exception of a single grain of isoferroplatinum or ferroan platinum, laurite–

erlichmanite is the only PGM occurring as micro-inclusions in chromite. (4) Nearly all of the PGM found in the chromitite are rich in S, *i.e.*, PGE sulfides or sulfarsenides. These features are generally consistent with those reported from chromitite layers in the Bushveld and Stillwater complexes (Von Gruenewaldt *et al.* 1986, Talkington & Lipin 1986).

The S-rich character of the PGE mineralization at Bol'shaya Varaka contrasts with the S-poor environment of the chromitite. Subsolidus re-equilibration between chromite and sulfide may have caused loss of Fe from the sulfide and relative enrichment in S in the associated sulfide assemblages; the formation of "free S$_2$" might be a possible consequence of this process (Von Gruenewaldt *et al.* 1986). Thus, local increase in sulfur fugacity, *f*(S$_2$), may have promoted the formation of sulfurian sperrylite at Imandra, along with the other S-bearing or S-rich PGM.

The PGM occur as cluster-like or chain-like microaggregates, or as separate tiny grains, all of which (up to 30–40 microgains) are enclosed within magnesiohornblende, edenite, talc and phlogopite. The PGM in these aggregates may transect the hydrous silicates (*e.g.*, Fig. 2B). Typically, grains of the PGM are located at the edge of chromite grains, implying that these PGM crystallized after the chromite. A subparallel orientation of the PGM grains and associated base-metal sulfides is locally observed; this texture also implies a late-stage precipitation of the PGM, which was controlled by the cleavage and fractures in the hydrous silicate(s). Such textures bear a resemblance to those reported for a "bonanza-type" hydrothermal PGE-mineralization from the Kirakkajuppura deposit in the Penikat complex, Finland (Barkov *et al.* 1999a).

The textural observations indicate that most of the PGM (namely sperrylite, unnamed Cu$_2$(Ni,Co)Pt$_3$S$_8$, rhodian sulfurian sperrylite, hollingworthite, nickelian platarsite, PGE-rich pyrite, daomanite, and cooperite) were deposited during deuteric alteration at a postmagmatic-hydrothermal stage of crystallization of the chromitite layer. The presence of Cl in this environment is evident from the high levels of Cl in apatite associated with the PGM (up to 3.45 wt.% Cl). The enrichment in volatile species presumably facilitated crystallization of the PGM. Though Pt-rich sulfides (cooperite and braggite) crystallize under dry conditions at submagmatic temperatures of $\leq$1000°C (Cabri *et al.* 1978), a Pt-rich sulfide has been successfully synthesized from a low-temperature solution at <100°C (Tarkian *et al.* 1996). Sperrylite has also been obtained by hydrothermal synthesis at 300°C (Tikhomirova & Chichagov 2000). Synthetic CuPt$_2$S$_4$ (monoclinic Cu$_2$Pt$_4$S$_8$), which may be related to unnamed Cu$_2$(Ni, Co)Pt$_3$S$_8$ from Imandra, was found to precipitate from low-temperature solutions at 350°C, and to form a rim around synthetic cooperite, PtS (Evstigneeva 1994).

Hydrothermal laurite–erlichmanite

Laurite–erlichmanite forms micro-inclusions in chromite at Bol'shaya Varaka, similarly to laurite from other chromitites in a variety of geological settings. However, these laurite inclusions are generally less abundant than the laurite–erlichmanite grains located in contact with chromite grain margins in hydrous silicates or enclosed within hydrous silicates. Also, the larger grains of laurite were observed at the chromite grain boundaries, but submicrometric laurite is also present in the cluster-like micro-aggregates of PGM within the Mg-rich hydrous silicates and in close association with the late-stage sperrylite, hollingworthite, Ru–Os–Ir-rich pyrite and unnamed $Cu_2(Ni,Co)Pt_3S_8$; the latter phase may occur intergrown with the erlichmanite–laurite. Thus, an interesting implication from these textural relationships is that laurite–erlichmanite forms part of the postmagmatic hydrothermal PGE mineralization in the chromitite layer at Imandra. This occurrence of hydrothermal laurite contrasts with the other reported occurrences worldwide, in which laurite is interpreted to be magmatic in origin. Recently, Brenan & Andrews (2001) summarized magmatic associations of laurite and showed experimentally that the maximum thermal stability of RuS_2 is indeed high (1275°C), consistent with crystallization at a magmatic temperature. However, it is known that results of experiments under "dry" conditions are not always applicable to ore deposits. For example, the maximum thermal stability of MoS_2 is also very high (1350°C; see Craig 1982); however, molybdenite commonly forms at a low temperature in environments rich in volatiles, such as alkali-metasomatized rocks (*e.g.*, Barkov *et al.* 2000). The strong enrichment in volatile species existing in the chromitite layer at Imandra presumably resulted in the delayed crystallization of laurite at lower temperatures. In general, the crystallization of laurite–erlichmanite in this chromitite layer probably was controlled by a level of $f(S_2)$, or by a combination of factors, such as $f(S_2)$ and temperature, rather than by temperature alone. The micro-inclusions of laurite (and laurite intergrown with the Pt_3Fe-type alloy) in chromite probably formed at a lower $f(S_2)$, where the other sulfide species of the PGM were not stable (*e.g.*, see Fig. 5 in Talkington & Lipin 1986). The character of primary zoning in the laurite–erlichmanite at Imandra (*i.e.*, relative enrichment of laurite in Os toward the rim) points to an increase in $f(S_2)$ in the environment during crystallization. This increase probably resulted in precipitation of the majority of the PGE sulfides at higher levels of $f(S_2)$ at a postmagmatic stage of crystallization. Also, As, which was incompatible during crystallization of chromite, must have accumulated at a postmagmatic stage, at which point the PGE sulfarsenides along with the late-stage PGE-sulfides deposited as interstitial phases in the chromitite.

REFERENCES

AMELIN, Y.V., HEAMAN, L.M. & SEMENOV, V.S. (1995): U–Pb geochronology of layered mafic intrusions in the eastern Baltic Shield: implications for the timing and duration of Paleoproterozoic continental rifting. *Precamb. Res.* **75**, 31-46.

BALASHOV, Y.A., AMELIN, Y.V., BAYANOVA, T.B., GANNIBAL, L.F., ZHANGUROV, A.A., KOSHCHEEV, O.A., RYUNGENEN, G.I., FEDOTOV, ZH.A., SHARKOV, I.V. & SHERSTENNIKOVA, O.G. (1990): The Imandra lopolith. *In* New Data on Geochronology and Isotope Geochemistry of Precambrian Rocks of the Kola Peninsula, **1**. Kola Science Center, Apatity, Russia (14-20; in Russ.).

BARKOV, A.Y., HALKOAHO, T.A.A., LAAJOKI, K.V.O., ALAPIETI, T.T. & PEURA, R.A. (1997): Ruthenian pyrite and nickeloan malanite from the Imandra layered complex, northwestern Russia. *Can. Mineral.* **35**, 887-897.

_____, _____, ROBERTS, A.C., CRIDDLE, A.J., MARTIN, R.F. & PAPUNEN, H. (1999a): New Pd–Pb and Pb–V oxides from a bonanza-type PGE-rich, nearly BMS-free deposit in the Penikat layered complex, Finland. *Can. Mineral.* **37**, 1507-1524.

_____, MARTIN, R.F., POIRIER, G. & MENSHIKOV, Y.P. (2000): Zoned tungstenoan molybdenite from a fenitized megaxenolith in the Khibina alkaline complex, Kola Peninsula, Russia. *Can. Mineral.* **38**, 1377-1385.

_____, THIBAULT, Y., LAAJOKI, K.V.O, MELEZHIK, V.A. & NILSSON, L.P. (1999b): Zoning and substitutions in Co–Ni–(Fe)–PGE sulfarsenides from the Mount General'skaya layered intrusion, Arctic Russia. *Can. Mineral.* **37**, 127-142.

BERLINCOURT, L.E., HUMMEL, H.H. & SKINNER, B.J. (1981): Phases and phase relations of the platinum-group elements. In *Platinum-Group Elements: Mineralogy, Geology, Recovery* (L.J. Cabri, ed.). *Can. Inst. Mining Metall., Spec. Vol.* **23**, 19-45.

BRENAN, J.M. & ANDREWS, D. (2001): High-temperature stability of laurite and Ru–Os–Ir alloy and their role in PGE fractionation in mafic magmas. *Can. Mineral.* **39**, 341-360.

CABRI, L.J., ed. (2002): The Geology, Geochemistry, Mineralogy, Mineral Beneficiation of the Platinum-Group Elements. *Can. Inst. Mining, Metall. Petroleum, Spec. Vol.* **54**.

_____ & FEATHER, C.E. (1975): Platinum–iron alloys. Nomenclature based on a study of natural and synthetic alloys. *Can. Mineral.* **13**, 117-126.

_____ & LAFLAMME, J.H.G. (1981): Analyses of minerals containing platinum-group elements. *In* Platinum-Group Elements: Mineralogy, Geology, Recovery (L.J. Cabri, ed.). *Can. Inst. Mining Metall., Spec. Vol.* **23**, 151-173.

_____, _____ & STEWART, J.M. (1977): Platinum-group minerals from Onverwacht. II. Platarsite, a new sulfarsenide of platinum. *Can. Mineral.* **15**, 385-388.

_____, _____, _____, TURNER, K. & SKINNER, B.J. (1978): On cooperite, braggite, and vysotskite. *Am. Mineral.* **63**, 832-839.

CRAIG, J.R. (1982): Survey of data on sulfide phase equilibria. *In* Sulfide Mineralogy (P.H. Ribbe, ed.). *Rev. Mineral.* **1**, 3-19.

DOKUCHAEVA, V.S., ZHANGUROV, A.A. & FEDOTOV, ZH.A. (1982): The Imandra lopolith – a new large layered intrusion in the Kola Peninsula. *Dokl. Akad. Nauk SSSR* **265**, 1282-1234 (in Russ.).

_____, _____ & _____ (1985): Distribution patterns of chromite and titanomagnetite deposits in the Imandra intrusion (Monchegorsk district). *In* Prognosis of Ore Deposits in the Kola Peninsula. Kola Branch of the USSR Academy of Sciences, Apatity, Russia (77-84; in Russ.).

EVSTIGNEEVA, T.L. (1994): An experimental investigation of platinum mineralization. *In* Geology and Genesis of Deposits of the Platinum Metals. Nauka Press, Moscow, Russia (257-263; in Russ.).

FURUSETH, S., SELTE, K. & KJEKSHUS, A. (1967): Solid solubility and structural properties of $PdAs_{2-x}Sb_x$, $PtP_{2-x}As_x$, $PtP_{2-x}Sb_x$, $PtP_{2-x}Bi_x$, $PtAs_{2-x}Sb_x$, $PtAs_{2-x}Bi_x$, $PtSb_{2-x}Bi_x$, $Pd_{1-m}Pt_mAs_2$, $Pd_{1-m}Pt_mSb_2$, $Pd_{1-m}Au_mSb_2$, and $Pt_{1-m}Au_mSb_2$. *Acta Chem. Scand.* **21**(2), 527-536.

GROSS, P.J. & JANSEN, M. (1994): Synthesis and crystal structure of $Cu_2Pt^{II}Pt^{IV}_3S_8$. *Z. anorg. allgem. Chem.* **620**(11), 1909-1914.

HULLIGER, F. (1964): Crystal structure and electrical properties of some cobalt group chalcogenides. *Nature* **204**, 644-646.

HWANG SONG-TZER, LEE MING-CHIH, TSAY MING-YIH & HUANG YING-SHENG (1994): Raman scattering of $Fe_xRu_{1-x}S_2$ mixed crystals. *Japan. J. Appl. Phys., Part 1,* **33**(11), 6203-6206.

IZOKH, A.E. & MAYOROVA, O.N. (1990): A rhodium-bearing sperrylite from the Nomgon complex (Mongolia). *Dokl. Akad. Nauk SSSR* **313**, 1212-1215 (in Russ.).

JOHAN, Z., OHNENSTETTER, M., SLANSKY, E., BARRON, L.M. & SUPPEL, D. (1989): Platinum mineralization in the Alaskan-type intrusive complexes near Fifield, New South Wales, Australia. 1. Platinum-group minerals in clinopyroxenites of the Kelvin Grove Prospect, Owendale Intrusion. *Mineral. Petrol.* **40**, 289-309.

JUZA, R., HULSMANN, O., MEISEL, K. & BILTZ, W. (1935): The systematic doctrine of affinity. LXVI. The sulfides of rhodium. *Z. anorg. allgem. Chem.* **225**, 369-385.

KOZLOV, M.T., LATYSHEV, L.N., DOKUCHAEVA, V.S., BARTENEV, I.S., SHLYAKHOVA, K.T., KOSTIN, S.M. & PAKHOMOVSKII, YA.A. (1975): A new type of chromite ore in quartz-bearing gabbronorites of the Monchegorsk area. *In* Basic and Ultrabasic Rocks of the Kola Peninsula and their Metallogeny. Kola Branch of the USSR Academy of Sciences, Apatity, Russia (108-125; in Russ.).

MAKOVICKY, E., MAKOVICKY, M. & ROSE-HANSEN, J. (2002): The system Fe–Rh–S at 900° and 500°C. *Can. Mineral.* **40**, 519-526.

MAKOVICKY, M., MAKOVICKY, E. & ROSE-HANSEN, J. (1992): The phase system platinum – iron – arsenic – sulfur at 850°C and 470°C. *Neues Jahrb. Mineral., Monatsh.*, 441-453.

OBERTI, R., UNGARETTI, L., CANNILLO, E. & HAWTHORNE, F.C. (1993): The mechanism of Cl incorporation in amphibole. *Am. Mineral.* **78**, 746-752.

PEREGOEDOVA, A. & OHNENSTETTER, M. (2002): Collectors of Pt, Pd and Rh in a S-poor Fe–Ni–Cu sulfide system at 760°C: experimental data and application to ore deposits. *Can. Mineral.* **40**, 527-561.

STONE, W.E., CROCKET, J.H. & FLEET, M.E. (1996): Platinum-group mineral occurrence associated with flow top amygdale sulfides in komatiitic basalt, Abitibi Greenstone Belt, Ontario. *Mineral. Petrol.* **56**, 1-24.

TALKINGTON, R.W. & LIPIN, B.R. (1986): Platinum-group minerals in chromite seams of the Stillwater complex, Montana. *Econ. Geol.* **81**, 1179-1186.

TARKIAN, M., EVSTIGNEEVA, T.L. & GORSHKOV, A. (1996): Synthesis of Pt- and Pd-sulphides in low temperature (85°C) solutions buffered by clay minerals and graphite: preliminary results. *Mineral. Petrol.* **58**, 71-78.

TIKHOMIROVA, V.I. & CHICHAGOV, A.V. (2000): Hydrothermal synthesis and crystallography of aurostibite ($AuSb_2$), sperrylite ($PtAs_2$) and geversite ($PtSb_2$). *Dokl. Akad. Nauk* **373**(3), 382-384 (in Russ.).

TIN, KUI-SHOU, HO, CHUN-HENG & CHENG, CHI-TAI (1981): Crystal structure of daomanite. *K'o Hsueh T'ung Pao* **26**(9), 554-557 (in Chinese).

TOLSTYKH, N.D., FOLEY, J.Y., SIDOROV, E.G. & LAAJOKI, K.V.O. (2002): Composition of the platinum-group minerals in the Salmon river placer deposit, Goodnews Bay, Alaska. *Can. Mineral.* **40**, 463-471.

VON GRUENEWALDT, G., HATTON, C.J., MERKLE, R.K.W. & GAIN, S.B. (1986): Platinum-group element – chromitite associations in the Bushveld complex. *Econ. Geol.* **81**, 1067-1079.

WOHLER, L., EWALD, K. & KRALL, H. (1933): The sulfides, selenides and tellurides of the six platinum metals. *G. Ber.* **66B**, 1638-1652.

YU, ZU-XIANG (1986): Some new minerals from platinum-bearing rocks in Yanshan and Tibet regions, China. *Bull. Inst. Geol., Chinese Acad. Geol. Sci.* **15**, 49-57 (in Chinese, with English abstr.).

_____ (2001): New data for daomanite. *Dizhi Xuebao* **75**(3), 396-399 (in Chinese).

_____, DING, KUI-SHOU & ZHOU, JIAN-XIONG (1978): Study on the new mineral daomanite. *Ti Chih Hsueh Pao* **52**(4), 320-325 (in Chinese).

APPENDIX 1. ANALYTICAL METHODS

Wavelength-dispersion (WDS) electron-microprobe analyses of hydrous silicates and chromite were carried out using a JEOL–733 electron microprobe. The operating conditions were 15 kV and 15 nA, and the following X-ray lines and standards were used: Si$K\alpha$, Ca$K\alpha$ (wollastonite), Mg$K\alpha$ (periclase), K$K\alpha$ (orthoclase), Na$K\alpha$ (jadeite), Al$K\alpha$ (synthetic Al_2O_3), Ti$K\alpha$ (rutile), Fe$K\alpha$, Cr$K\alpha$, V$K\alpha$, Ni$K\alpha$, Mn$K\alpha$ (pure elements), and Cl$K\alpha$ (KCl).

The WDS analysis of a PGE-rich pyrite was made using a JEOL–733 instrument operated at 20 kV and 15 nA. A finely focused beam and the following lines and standards were used: Ru$L\alpha$, Pt$L\alpha$, Os$L\alpha$, Ir$L\alpha$ (pure metals), Fe$K\alpha$, and S$K\alpha$ (FeS_2). The raw data were ZAF-corrected on line.

Energy-dispersion (EDS) electron-microprobe analyses of hydrous silicates, base-metal sulfides and various PGM were carried out at 15 kV and 1.7 nA, using a JEOL JSM–6400 scanning-electron microscope (SEM) equipped with a LINK eXL energy-dispersion spectrometer. The $K\alpha$ line and the following set of standards were used for hydrous silicates: SiO_2, apatite, MgO, orthoclase, jadeite, Al_2O_3, KCl, and pure Ti, Fe, and Cr. Most of the reported compositional data are based on results of quantitative SEM/EDS analyses; the choice of this method was influenced by the very small grain-size of the PGM. The following set of standards was used for the PGM: Pt, Ru, Os, Ir, Pd (pure metals), Rh (synthetic RhSb), Co, Ni, Cu (pure metals), Fe, S (FeS_2), and As ($PtAs_2$). The *M* X-ray line was used for Pt and Ir. The *L* line was used for Ru, Rh, and As. The *K* line was used for Fe, Co, Ni, Cu, and S. The spectra were processed by a LINK ISIS on-line program. If the analyses of PGM gave a total higher than 102 wt.% or slightly lower than 98 wt.%, they were normalized to 100%. The counting periods were 100 s, and a finely focused beam (*ca.* 1 μm) was used in all of the EDS analyses.